Research Square

Preprints are preliminary reports that have not undergone peer review.
They should not be considered conclusive, used to inform clinical practice,
or referenced by the media as validated information.

Potential Metal Chelating Ability of Mycosporine-Like Amino Acids: A Computational Research

Tereza Varnali (varnali@boun.edu.tr)
Bogazici University https://orcid.org/0000-0001-7424-6458
Mert Bozoflu
Bogazici University
Hüseyin Şengönül
Bogazici University
Seher İ. Kurt
Bogazici University

Research Article

Keywords: Mycosporine-like amino acids, metal chelation, iron- MAA complexes, calcium-MAA complexes, molecular modeling, DFT.

Posted Date: July 7th, 2021

DOI: https://doi.org/10.21203/rs.3.rs-657747/v1

License: This work is licensed under a Creative Commons Attribution 4.0 International License.
Read Full License

Version of Record: A version of this preprint was published at Chemical Papers on January 30th, 2022.
See the published version at https://doi.org/10.1007/s11696-021-02014-x.

Abstract

Mycosporine-like amino acids (MAAs) are low molecular-weight (<400 Da) water soluble secondary metabolites that are attributed many functions such as antioxidants, compatible solutes, nitrogen reservoirs and especially, photostable UV-protectants. Recently, they are attracting attention due to their biotechnological and industrial potential for anti-aging and wound healing properties as well. In this study, we explored the metal chelating capacity of selected MAAs (4-deoxygadusol, mycosporine-glycine, mycosporine-taurine, palythine, poryphyra-334, shinorine, mycosporine-2-glycine and euhalothece-362) making use of dft calculations. We report model structures of ferrous and ferric ion-MAA complexes and their binding affinities in relation to their structural differences and multiple sites available for chelation on the MAAs. We also investigated calcium ion complexes for mycosporine-glycine, shinorine, porphyra-334 and mycosporine-2-glycine. Our findings support previous suggestions made to explain some experimental results obtained in earlier studies on MAAs. Lastly, we briefly mention the findings in the context of early life and hence relevance to astrobiology.

Introduction

Mycosporine-like amino acids (MAAs) were originally found in 1960s [1] and have attracted attention ever since. There are many reviews written about their structures, biosynthesis [2–4]; roles such as antioxidant molecules, compatible solutes, nitrogen reservoirs; protection against UV-radiation, dessication or thermal stress, [5–7] as well as their biotechnological and industrial potential as natural sunscreens, anti-photoaging molecules, stimulators of skin renewal and functional ingredients of UV-protective biomaterials [8–11]. They are widely distributed in various organisms all over the globe [12]. MAAs are low molecular-weight (< 400 Da) water soluble compounds. They absorb UV radiation with λ_{max} 310 to 365 nm and high molar absorptivity. Therefore, they are generally considered to be UV absorbing pigments and regarded as ‘multipurpose’ secondary metabolites due to their additional roles listed above [5]. MAAs structures consist of a cyclohexenone or cyclohexenimine ring substituted with a methoxy group at C2, a hydroxy group and a hydroxymethyl group at C5 and are conjugated to an amino compound (generally glycine) at C3 of the ring (Fig. 1) [2, 13]. A second amino acid (amino alcohol or enamino group may be substituted at C1 of the ring.

MAAs may be extracellular as well as intracellular [14]. Hu et al. report shinorine to be exclusively located in the extracellular matrix in cyanobacteria *Microcystis aeruginosa* PCC 7806 and that it does not play a major role in UV protection but may be involved in extracellular matrix formation and cell to cell interaction [15]. According to Ingalls et al, a significant amout of organic matter bound to diatom frustules comprise of MAAs [16]. The cyanobacterium *Trichodesmium spp* [17], dinoflagellate *Lingulodinium polyedra* [18], and dinoflagellate *Prorocentrum micans* [19] actively secrete MAAs into the surrounding water during surface blooms.

Cyanobacteria (CB) are very diverse and ubiquitous on earth [20]. They are the most studied organisms among those found to produce MAAs (ie. prokaryotes, eucaryotic algae, invertebrates, dinoflgellates,

vertebrates, bacteria and yeast) [21]. CB most likely evolved from anoxygenic phototrophs [22]. Hickman-Lewis et al show that bacteria and archea fluorished together in Earth's earliest ecosystems 3.5 to 3.2 Ga [23]. Garcia-Pichel et al. estimate the most recent common ancestor of the phylum CB existed ~ 3.6 Ga [24]. The development of oxygenic photosynthesis by CB caused the great oxygenation event (GOE) of the atmosphere during the early Proterozoic, 2.5–2.3 Ga, and led to evolutionary changes on earth [25]. Consequently, they were the first taxa to adapt to the oxidative stress with existing systems [26]. CB could have used MAAs as antioxidants as well as photoprotectants [22].
A gene cluster for MAA synthesis, homologus to those identified from CB, was recently confirmed for two strains of actinobacteria. These bacteria have no photosynthesis ability and live in terrestrial environments. It was the first confirmation of a gene cluster for MAA production from Gram-positive bacteria.[27]. Actinobacteria, similarly to CB are very common and diverse (from anaerobic, unicellular organisms to aerobic, filamentous, and spore-forming lineages) [28]. They predate the GOE and together with CB and Deinococcus share a common ancestor [29].

Photoferrotrophy, a form of anoxygenic photosynthesis (use of light as energy source and ferrous ion as electron donor), is one of the oldest photoautotrophic metabolisms on Earth [30]. Mechanistically, the biochemical pathway for the conservation of energy coupled to the oxidation of iron is still poorly understood [31]. Photoferrotrophs display mechanisms preventing cell encrustation with oxidized iron [32–34. Gauger et al. demonstrated that the anoxygenic phototrophic Fe(II) oxidizers *Rhodopseudomonas palustris* strain TIE-1 (purple non sulfur bacteria PNSB) and *Rhodobacter ferrooxidans* strain SW2 (prockaryote - bacterium) form nanometer-sized grains of ferrihydrite loosely attached to the cell surfaces to protect themselves from UV irradiation [35]. In environments where Fe(II) was abundant, the production of Fe(III) minerals may have constituted UVR protection, an early survival strategy. Properties of such Fe(III) minerals include the absorption of light in the low UV range (< 400 nm), although visible light (~ 390–700 nm) is still transmitted [35]. Kolo et al report iron encrusted microbial like structures (MLS) on surfaces of hematite in a banded iron formation (BIF). They state "original cells" could have been Fe III reducing bacteria or "other" and that pitting found on surfaces might have resulted due to dissolution via iron chelators [36].

Iron amino acid chelates, such as iron glycinate chelates (Ferrous bis-glycinechelate, ferric tris-glycine chelate, ferric glycinate, and ferrous bis-glycinate hydrochloride), were developed to be used as food fortificants and therapeutic agents in the prevention/ treatment of iron deficiency anemia and are available commercially[37]. Ferrous glycinate nanoliposomes may be fit for the oral administration of ferrous glycinate and may be used for the fortification of foodstuffs [38]. Iron amino acid chelates can be used as an alternative for Fe-EDTA to supply iron in nutrient solutions for plant growth [39]. MAAs have at least one amino acid (usually two) and they are antioxidants (readily donate electrons) [7]. They seem to be ideal candidates to chelate iron.

There are a few quantum calculational theoretical studies carried out at the molecular level on MAAs. Klisch et al., in their experimental and calculational studies on porphyra-334 depict the absolute configuration at the stereogenic center of the ring (C5) as *S*; *E* configuration at the imino moiety; and an

exceptionally high proton affinity (265.7 kcal/mol) [40]. The photoprotection mechanism of palythine as ellucidated by Sampedro is a very rapid deactivation of the excited state in which light energy is dissipated as heat [41]. Losantos et al describe a similar mechanism for highly photostable Gadusol [42]. Matsuyama et al. reveal the pH-independent charge-resonance mechanism of shinorine and related MAAs to be responsible of UV-protection [43]. Orfanoudaki et al, in a very recent study, report the absolute configuration of 14 MAAs and show that all of the tested MAAs have the ability to inhibit collagenase. They refer to two studies that hypothesize MAAs could play a role due to chelation of iron and calcium for this unknown mechanism of inhibition [44]. In the first paper, Volkman etal., state that the MAA "Euthalece-362 with its four hydroxyl groups together with the alanine carboxyl group, may act as an iron chelator" [45]. In the second paper by Tarasuntisuk et al, it is stated that mycosporine-2-glycine's inhibitory activity on protein crosslinking may have been due to the chelation of calcium ions [46].

In this study, we present the iron chelating ability of selected MAAs. We modeled iron-MAA complexes for the MAAs shown in Fig. 1 **(** including 4-deoxygadusol, mycosporine-glycine, mycosporine-taurine, palythine, poryphyra-334, shinorine, mycosporine-2-glycine and euhalothece-362). We also examined SH, PR, M2G, and MG for their calcium chelating capacity to compare with findings in the paper referred above [44, 46].

Modeling And Computations

Previous quantum calculational theoretical studies carried out on MAAs provide most of the structural information required to model MAAs at the molecular level, ie: geometries, conformations, isomers, absolute configurations, zwitterions, etc.[40-44]. We modeled ferrous and ferric iron-MAA complexes both for the neutral forms and the anionic forms of the selected MAAs**.** The selected MAAs are 4-deoxygadusol (**4DG**), the common precursor of all MAAs with the oxo-ring; mycosporine-glycine (**MG**) with the oxo-ring and glycine as the substituent at C3; mycosporine-taurine (**MT**) with the oxo-ring and taurine on C3; palythine (**PT**) with the imino core ring and glycine substituent on C3; poryphyra-334 (**PR**), shinorine (**SH**), mycosporine-2-glycine (**M2G**), all three with glycine substituent at C3 and different amino acids (threonine, serine, glycine respectively) substituted at C1 as second substituents; and euhalothece-362 (**EU**), with an enylimino group at C1 and alanine substituted at C3.

4DG, represents the basic structure of the conjugated oxo-ring. The numbering used through out this work is shown on the figure for 4DG **(Fig 2)**. The anion (enolate form) of 4DG , 4-deoxygadusolate (**4DG-ate**), dominates the acid-base equilibrium in water. This structure delocalizes the charge at pH 7 as shown in **Fig. 2** and is protonated to the neutral form under acidic conditions [42,43]. C5 is the stereogenic center on the ring. The protonation of the oxygen on C1 produces the stereoisomer (mirror image) of **4DG-ate** obtained by the protonation of the oxygen on C3 (the priority numbers of the groups surrounding the stereogenic center C5 change). Therefore, both stereoisomers are equally expected to be present under acidic conditions. Iron is separately placed in two different locations, Position 1 or Position 2 (**Fig. 2)** to test iron chelation of 4DG. These two positions become equivalent for **4DG-ate** due to its charge-resonance delocalization.

MG is derived from 4DG. It has a glycine moiety on C3. The absolute configuration of C5 is defined as S [47]. MG has three positions in which iron may be tested for chelation. Position 1 is the same as that in 4DG. The second position is in between the methoxy oxygen and the carboxyl group, also in close proximity to the nitrogen. The third position is between the carboxyl group and the two hydroxy groups on C5 (**Fig. 3**). **MG** is in its zwitterionic nature in the range pH 4-10 and delocalizes the charge over 5 atoms, from O to N (**Fig. 3**)[43]. It is not clear whether the neutral or zwitterionic forms of the MAA structures are active *in vivo* [41]. Therefore, both the neutral forms and the anions of their zwitterionic forms are studied (**Fig. 3**). A H^+ ion (either on C1-O or on C3-N, each separately) is removed from the zwitter ion and an iron ion is placed in Position 1 (P1) , Position 2 (P2) or Position 3 (P3) to form an **iron-MG-ate** chelate model. Also, each form is modeled both as a ferrous and a ferric ion chelate. This procedure is carried out for all of the MAAs**.**

MT has the same core structure as MG but with a taurine moiety on C3. The longer chain in taurine compared to glycine (two $-CH_2-$ groups between the nitrogen and the sulfur) may allow the $-SO_3H$ (or $-SO_3^-$ in the zwitterion) group to reach a larger conformational space. The absolute configuration of MT is undefined but it is derived directly from 4DG therefore we adopted the *S* configuration at C5. **PT** structure is similar to that of MG. The only difference between them is the replacement of the keto group with an imine group (**Fig. 4**). It represents the imino core ring. **SH** has a serine, **PR** has a threonine moiety on C1. They both have E configuration at the imino moiety, absolute configuration *S* at C5 , and another chiral carbon (*S*) bound to the imino nitrogen with a carboxyl group on it [40,44]. The carbon that bears the methyl group in **PR** has absolute configuration *R* [40]. **PT**, **SH**, **PR** and **M2G** are all in zwitterionic nature in the range pH 4-10 [43,44] and delocalize the charge in the zwitterionic form as shown in **Fig. 4**. **EU** has a 2,3-dihydroxyprop-1-enylimino group at C1 and alanine substituted at C3 [45]. Its charge-resonance delocalization is extended to seven atoms (**Fig. 1).** The absolute configuration at C5 being undefined. We chose to model the S form like the rest of the MAAs in this study.

We then modeled MG,SH, PR, and M2G with the same strategy for their calcium ion complexing ability.

Hybrid DFT methods offer excellent performance in the prediction of geometries of small and medium size molecules. Our aim being the search of good geometries to model potential iron-chelates for a series of MAAs that have already been studied both experimentally and calculationally, our choice is the most cost-effective method B3LYP in conjuction with 6-31G (d p) basis set. The geometry of each iron-MAA complex structure modeled is fully optimized and a frequency calculation is carried out to ensure true minimum (no imaginary frequency). Gas phase calculations are run for isolated structures at 298 K, 1 atm. Calculations are carried out making use of the Gaussian'09 program package [48] for iron complexes and Gaussian'16 for calcium complexes.

The metal affinities are calculated according to the following equations

$$E_{\text{metal affinity}} = E_{\text{M-MAA complex}} - (E_M + E_{MAA})$$

$E_{metal\ affinity} = E_{M\text{-}MAA\text{-}ate\ complex} - (E_M + E_{MAA\text{-}ate})$

in which M is the metal ion = Fe^{2+}, Fe^{3+}, Ca^{2+}; MAA stands for neutral forms and MAA-ate stands for the anion of the zwitter ionic forms of MAAs.

Results And Discussion

All of our MAA models are in accordance with the structure reported for palythine by Furusaki et al "with the six membered ring in an envelope form, C5 out of the plane formed by the other five carbon atoms, the –OH group on C5 in the axial and the -CH_2OH group in the equatorial position" [49]. The methyl group on the methoxy substituent on C2 is synperiplanar with the –OH group on C5 or rotated depending on the position the metal chelation occurs. The methyl group tends to move away from the metal ion. The procedure we applied to model iron-MAA complexes implies that the iron cation either replaces the H^+ ion removed at P1 / P2 or prefers to bind at P3. To rephrase it for the iron-MAA-ate complexes, the carboxylic acid group releases the H^+, the zwitter ion forms and the ferrous or ferric iron ion replaces the H^+ ion (at P1 or P2) or binds at P3. We tested different multiplicities for the ferrous/ferric complexes formed at different positions to find out if there are incidences at which the energy of the complex formed is lower than the one with the high spin. The calculated energies for the Fe^{2+} complexes with multiplicity 5 and Fe^{3+} complexes with multiplicity 6 were those with the lowest energies of all the obtained complexes. From here on, "Fe^{2+} " stands for ferrous ion with multiplicity 5 and "Fe^{3+} " stands for ferric ion with multiplicity 6. The results and data for optimized structures of the most stable ferrous and ferric iron complexes are presented in **Table 1**. The most stable (lowest energy) iron-MAA and iron-MAA-ate chelates obtained are shown in **Fig. 5**. A concise summary of the theoretical work (Energies, Metal affinities, complex forming bond lengths and important metal to closest atoms distances) is presented in **Table S1**.

4DG binds Fe^{2+} at P1 with a covalent bond to the carbonyl oxygen. We were not able to obtain an Fe^{3+} complex for 4DG. 4DG-ate binds both Fe^{2+} and Fe^{3+} at the only available position (P1 and P2 become equivalent as explained above).

MG, PT, M2G, EU all bind Fe^{2+} at P2 with a covalent bond to the nitrogen on C3. MT binds Fe^{2+} at P2 with a covalent bond to a sulfonic oxygen. SH and PR bind Fe^{2+} at P1 with a covalent bond to the nitrogen on C1. MG binds Fe^{3+} covalently to the oxygen of the carboxylic acid group at P3 but we could not model an Fe^{3+} complex for any of the other MAAs.

MG-ate, PT-ate, M2G-ate, EU-ate all bind Fe^{2+} at P2 (for M2G, P1= P2) with a covalent bond to the carboxyl oxygen. Our attempts to model an Fe^{2+} MT-ate complex at P2 resulted in a non-covalent complex with distances comparable to those of covalent bond(s) to the nitrogen, methoxy oxygen and a sulfonic oxygen (Table S1). SH-ate and PR-ate bind Fe^{2+} at P1 with a covalent bond to the carboxyl oxygen.

Similarly, MG-ate, PT-ate, M2G-ate bind Fe^{3+} at P2 (for M2G, P1= P2) with a covalent bond to the carboxyl oxygen and a second covalent bond to the nitrogen on C3. MT-ate binds Fe^{3+} at P2 with two covalent bonds to sulfonyl oxygens and a third covalent bond to the nitrogen on C3. EU-ate binds Fe^{3+} at P2 with a covalent bond to the carboxyl oxygen. SH-ate, and PR-ate bind Fe^{3+} at P1 with a covalent bond to the carboxyl oxygen and a second covalent bond to the nitrogen on C1. All attempts to bind iron at P3 failed for MG (except for $[Fe(MG)^{3+}]$, MG-ate, MT, MT-ate, PT, PT-ate. Therefore we did nor search further at P3 for the rest of the MAAs.

These observations show that the best position for iron binding is P2. The carboxylic acid (–COOH or $–COO^-$) group of the MAA (or MAA-ate), the methoxy oxygen and the nitrogen on C3 act as three tethers for chelation when Fe^{2+} is at P2. The methoxy oxygen seems to play a role through Coulombic forces. Unlike the rest of the series, P1 is the best binding position for SH, SH-ate, PR and PR-ate. The reason may be the lower pKa of the serine and the threonine moieties at P1 compared to pKa of glycine at P2 and /or the presence of the –OH group on serine and threonine acting as a fourth tether at P1. Coulombic forces with the methoxy oxygen seem to be influential both at P1 and P2 for Fe^{3+} binding as well.

The order of affinities for ferrous ion are 4DG **<** MG < PT < M2G **<** MT < EU < PR **<** SH and 4DG-ate **<** MG-ate **<** PT-ate < M2G-ate <EU-ate **<** SH-ate < PR-ate.Similarly the order of affinities for ferric ion is 4DG-ate **<** MG-ate < PT-ate **<** MT-ate < M2G-ate **<** SH-ate < EU-ate < PR-ate.

To summarize and generalize, 4DG, and all the MAAs studied bind Fe^{2+} both in the neutral form and the enolate form. They bind Fe^{3+} only in the enolate form (only MG binds Fe^{3+} in the neutral form too). All the MAAs studied bind iron with three tethers at P2 except SH and PR. SH and PR have amino acids substituted at C1 which are more acidic than glycine and have an –OH group on the amino acid that may act as a fourth tether at P1.

Our results support Volkman et al's suggestion that Euhalothece-362 may act as an iron chelator [45] and Tarasuntisuk et al's observed chelating activity for M2G [46].

The results and data for optimized structures of the most stable Ca^{2+} complexes are presented in **Table 2**. The calcium complexes are non-covalent complexes. MG chelates Ca^{2+} at P2 in close proximity to nitrogen, methoxy oxygen and carboxylic oxygen. M2G (P1=P2) chelates Ca^{2+} exactly like MG. SH and PR chelate Ca^{2+} at P1 in between the nitrogen, methoxy oxygen, carboxylic oxygen and the hydroxyl group on serine or threonine respectively. The affect of the fourth tether observed for iron complexes of SH and PR is observed for the calcium complexes as well. MG-ate, M2G-ate, SH-ate and PR-ate all chelate Ca^{2+} at P3 by four oxygen atoms, namely the two oxygens of the carboxyl group and the two oxygens of the hydroxy and methylhydroxy groups on C5. The common element in the pool for those tested at P3 is MG-ate. Comparison of iron chelating to calcium chelating behavior of MG-ate reveals that P3 may be preferable to P1/P2 for non-covalent chelation.

The order of affinities for Ca^{2+} are MG ~ M2G < PR <SH and MG-ate < M2G-ate <SH-ate < PR-ate. Our results support that MAAs have the chelating ability of metals referred to by Orfanoudaki et al [44].

The outcome of this computational research is highly relevant to life on early earth and hence to astrobiology. CB and Actinobacteria share a common ancestor and predate GOE [29]. MAAs could have been synthesized by their most ancient strains and could have served for iron acquisition during anoxic times. CB, being the first taxa to adapt to the oxidative stress with existing systems [26] could have used MAAs as antioxidants as well as metal chelators. Photoferrotrophs' mechanisms preventing cell encrustation with oxidized iron [32-34] may have been be due to extracellular MAAs. MAAs have the potential to serve bacteria as iron-chelators for the purpose of screening UVR (as colloid, on extracellular polymeric saccharides, or intracellularly). Further more, bacteria may also potentially utilize MAAs intracellularly or extracellularly for iron transport, solubilization, mobilization and storage purposes.

Conclusion

In this study, we discuss the potential iron chelating ability for 4-deoxygadusol, mycosporine-glycine, mycosporine-taurine, palythine, poryphyra-334, shinorine, mycosporine-2-glycine and euhalothece-362 and calcium chelating ability for poryphyra-334, shinorine, mycosporine-2-glycine and mycosporine-glycine in relation to their molecular structure. Our results show stable metal complexed MAA structures. Our findings support suggestions made in the literature on the potential chelating ability of MAAs to explain some experimental results obtained in previous MAA studies. Lastly, we briefly mention the findings in the context of early life and relevance to astrobiology. To the best of our knowledge, this is the first data report on MAAs metal chelation ability and ascribes them a new role (or maybe their very ancient role) as " metal chelators".

Declarations

Acknowledgements

This work has been funded by Bogazici University Research Funds, Project No: 15B05P4.

TV thanks Igor Brown for the discussions and exchange of ideas (private communication).

Funding

Bogazici University Research Funds, Project No: 15B05P4.

Conflicts of interest/competing interests

The authors declare that they have no conflict of interest/ competing interests.

Availability of data and material:

SI (Supportive Information) provided

Code availability

Not applicable

Authors contributions: (optional)

Tereza Varnali contributed to the study conception and design. Data collection and analysis were performed by Tereza Varnali, Mert Bozoflu, Hüseyin Şengönül and Seher I. Kurt. The first draft of the manuscript was written by Tereza Varnali and all authors commented on previous versions of the manuscript. All authors read and approved the final manuscript.

Ethics approval

Not applicable

Consent to participate

Not applicable

Consent for publication

Not applicable

References

1. ŘezankaT, TeminaM, TolstikovAG, DembitskyVM (2004) Natural microbial UV radiation filters - Mycosporine-like amino acids. Folia Microbiologica49: 339–352 https://doi.org/10.1007/BF03354663

2. Sinha RP, Häder DP (2008) UV-protectants in cyanobacteria. Plant Science 174: 278–289

3. S.P. Singh, S. Kumari, R.P. Rastogi, K.L. Singh, R. P. Sinha (2008) Mycosporine-like amino acids: chemical structure biosynthesis and significance as UV- absorbing/ screening compounds. Indian Journal of experimental biology 46:7-17

4. Pathak J, Ahmed H, Rajneesh, Singh SS, Hader DP (2019) Genetic regulation of scytonemin and mycosporine-like amino acids (MAAs) biosynthesis in cyanobacteria. Plant Gene 17: 10072

5. Oren A, Gunde-Cimerman N (2007) Mycosporines and Mycosporine-Like Amino Acids: UV protectants or multipurpose secondary metabolites? FEMS Micobiol. Lett 269:1-10

6. Wada N, Sakamoto T, Matsugo S (2013) Multiple Roles of Photosynthetic and Sunscreen Pigments in Cyanobacteria Focusing on the Oxidative Stress. Metabolites 3: 463-483 doi:10.3390/metabo3020463

7. Wada N, Sakamoto T, Matsugo S (2015) Mycosporine-Like Amino Acids and Their Derivatives as Natural Antioxidants. Antioxidants 4: 603-646 doi:10.3390/antiox4030603

8. Rastogi, R.P.; Sinha, R.P. (2009) Biotechnological and industrial significance of cyanobacterial secondary metabolites Biotechnol. Adv 27: 521–539

9. Chrapusta E, Kaminski A, Duchnik K, Bober B, Adamski M, Bialczyk J (2017) Mycosporine-Like Amino Acids: Potential Health and Beauty Ingredients. Mar. Drugs 15: 326

10. Fuentes-Tristana S, Parra-Saldivara R, Iqbala HMN, Carrillo-Nievesb D (2019) Bioinspired biomolecules: Mycosporine-like amino acids and scytonemin from *Lyngbya* sp. with UV-protection potentialities. Journal of Photochemistry & Photobiology, B: Biology 201:111684

11. Rosic NN (2019) Mycosporine-Like Amino Acids: Making the foundation for organic personalised sunscreens. Mar. Drugs 17:638 Review doi: 10.3390/md17110638

12. Shick JM, Dunlap WC (2002) Mycosporıne-lıke amino acids and related gadusols:Biosynthesis, Accumulation, and UV-Protective Functions in Aquatic Organisms. Annu. Rev. Physiol. 64:223–62.

13. Simeonov A, Michaelian K (2017) arXiv:1702.03588v2[physics.bio-ph]

14. Böhm GA, Pfleiderer W, Böger P, Scherer S. (1995) Structure of a novel oligosaccharide-mycosporine-amino acid ultraviolet A/B sunscreen pigment from the terrestrial cyanobacterium Nostoc commune. J Biol Chem. 270:8536–9

15.Hu C, Völler G, Roderich Süßmuth, Dittmann E, Kehr JC. (2015) Functional assessment of mycosporine-like amino acids in *Microcystis aeruginosa* strain PCC 7806. Environmental Microbiology 17:1548–1559.

16. Ingalls AE, Whitehead K, Bridoux, M. C. (2010) Tinted windows: The presence of the UV absorbing compounds called mycosporine-like amino acids embeddedin the frustules of marine diatoms. Geochim. Cosmochim. Acta, **74**, 104-115

17. Subramaniam A, Carpenter EJ, Karentz D, Falkowski PG (1999) Bio-optical properties of the marine diazotrophic cyanobacteria *Trichodesmium spp.* I. Absorption and photosynthetic action spectra. Limnol. Oceanogr., 44(3): 608–617

18. Vernet M, Whitehead K ((1996) Release of ultraviolet-absorbingcompoundsby the red-tide dinoflagellate *Lingulodinium polyedra*. Marine Biology 127:35-44.

19. Tilstone GH, Airs RL, Martinez-Vicente V, Widdicombe C, Llewellyn C (2010) High concentrations of mycosporine-like amino acids and colored dissolved organic matter in the sea surface microlayer off the Iberian Peninsula. Limnol. Oceanogr., 55(5): 1835–1850 doi:10.4319/lo.2010.55.5.1835

20 Shih PM, Wu D, Latifi A, Axen SD, Fewer DP, Talla E, Calteau A, Cai F, Tandeau de Marsac N, Rippka R, Herdman M, Sivonen K, Coursin T, Laurent T, Goodwin L, Nolan M, Davenport KW, Han CS, Rubin EM, Eisen JA, Woyke T, Gugger M, Kerfeld CA (2013) Improving the coverage of the cyanobacterial phylum using diversity-driven genome sequencing. PNAS 110 (3): 1053–1058

21. Jain S, Prajapat G, Abrar M, Ledwani L, Singh A, Agrawal A (2017) Cyanobacteria as efficient producers of mycosporine-like amino acids J Basic Microbiol 57:715-727

22. Shih MP (2019) Early Cyanobacteria and the innovation of microbial sunscreens mBio 10:e01262-19

23. Hıckman-Lewıs K, Westall F, Cavalazzı B, (2020) Diverse communıtıes of bacteria and archaea flourished in palaeoarchaean (3.5–3.3 ga) mıcrobıal mats Palaeontology 1-27

24. Garcia-Pichel F, Lombard J, Soule T,Dunaj S, Wu SH, Wojciechowski MF (2019) Timing the evolutionary advent of cyanobacteria and the later Great Oxidation Event using gene phylogenies of a sunscreen. mBio 10:e00561-19. doi:10.1128/mBio.00561-19

25. Schirrmeister BE, Gugger M, Donoghue PCJ (2015) Cyanobacteria and the great oxidation event: evidence from genes and fossils Palaeontology, 1–17. doi: 10.1111/pala.12178

26. FischerW, HempJ, Valentine JS (2016) How did life survive Earth's great oxygenation? Current Opinion in Chemical Biology31:166-178. doi:10.1016/j.cbpa.2016.03.013.

27. Miyamoto KT, Komatsu M, Ikeda H (2014) Discovery of Gene Cluster for Mycosporine-Like Amino Acid Biosynthesis from *Actinomycetales* Microorganisms and Production of a Novel Mycosporine-Like Amino Acid by Heterologous Expression. Applied and Environmental Microbiology 80:5028–5036.

28. Lewin GR, Carlos C, Chevrette MG, Horn HA, McDonald BR, Stankey RJ, Fox BG, Cameron R. Currie CR (2016) Evolution and Ecology of *Actinobacteria* and Their Bioenergy Applications. Annu Rev Microbiol. 70: 235–254. doi: 10.1146/annurev-micro-102215-095748

29. Battistuzzi FU, Feijao A, Hedges SB (2004) A genomic timescale of prokaryote evolution: insights into the origin of methanogenesis, phototrophy, and the colonization of land BMC Evol Biol. 4:44. doi:10.1186/1471-2148-4-44

30. Camacho A, Walter XA, Picaz0 A, Zopfi J (2017) Photoferrotrophy: Remains of an ancient Photosynthesis in Modern Environments. Front Microbiol. 8: 323.

31. Floyd MAM, Williams AJ, Grubisic A, Emerson D (2019) Metabolic Processes Preserved as Biosignatures in Iron-Oxidizing Microorganisms:Implications for Biosignature Detection on Mars, Astrobiology 19:40-52 doi: 10.1089/ast.2017.1745

32. Miot J, Benzerara K, Obst M, Kappler A, Hegler F, Schäedler S, Bouchez C, guyot F, Morin G (2009) Extracellular iron biomineralization by photoautotrophic ironoxidizing bacteria. Appl. Environ.

Microbiol. 75, 5586–5591 doi: 10.1128/AEM.00490-09

33. Saraiva IH, Newman DK, Louro RO (2012) Functional characterization of the FoxE iron oxidoreductase from the photoferrotroph *Rhodobacter ferrooxidans* SW2. J. Biol. Chem.287, 25541–25548 doi: 10.1074/jbc.M112.360636

34. Wu W, Swanner ED, Hao L, Zeitvogel F, Obst M, Pan Y, Kappler A (2014) Characterization of the physiology and cell–mineral interactions of the marine anoxygenic phototrophic Fe(II) oxidizer *Rhodovulum iodosum*–implications for Precambrian Fe(II) oxidation. FEMS Microbiol Ecol88, 503–515

doi: 10.1111/1574-6941.12315

35. Gauger T, Konhauser K, Kappler A(2015) Protection of phototrophic iron(II)-oxidizing bacteria from UV irradiation by biogenic iron(III) minerals: Implications for early Archean banded iron formation. Geology 43(12):1067–1070 doi:10.1130/G37095.1

36. Kolo K, Konhauser K, Krumbein WE, Ingelgem YV, Hubin A, Claeys P (2009) Microbial Dissolution of hematite and associated cellular fosilization by reduced iron phases: A study of ancient microbe-mineral surface interactions. Astrobiology 9(8): 777–796 doi:10.1089/ast.2008.0263

37. Hertrampf E, Olivares M (2004) Iron amino acid chelates. Int J Vitam Nutr Res, 74(6): 435-43. doi: 10.1024/0300-9831.74.6.435.

38. Ding B, Zhang X, Hayat K, Xia S, Jia C, Xie M, Liu C (2011) Preparation, characterization and the stability of ferrous glycinate nanoliposomes. Journal of Food Engineering 102(2): 202-208

39. Ghasemi S, Khoshgoftarmanesh AH, HadadzadehH, Jafari M (2012) Synthesis of Iron-Amino Acid Chelates and Evaluation of Their Efficacy as Iron Source and Growth Stimulator for Tomato in Nutrient Solution Culture. Journal of Plant Growth Regulation 31:498–508

40. Klisch M, Richter P, Puchta R, Hader DP, Bauer W (2007) The stereostructure of Porphyra-334: An experimental and calculational NMR investigation. Evidence for an efficient 'proton sponge'. Helvetica Chimica Acta 90: 488-509

41. Sampedro D (2011) Computational exploration of natural sunscreens. Phys Chem Chem Phys 13:5584-5586

42. Losantos R , Churio MS, Sampedro D (2015) Computational exploration of the photoprotective potential of Gadusol. Chemistry Open 4:155-16

43. Matsuyama K, Matsumoto J, Yamamoto S, Nagasaki K, Inoue Y, Nishijima M, Mori T (2015) pH-Independent Charge Resonance Mechanism for UV Protective Functions of Shinorine and Related Mycosporine-like Amino Acids. J Phys Chem A 119(51):12722-12729

44. Orfanoudaki M, Hartmann A, Alilou M, Gelbrich T, Planchenault P, Derbre S, Schinkovitz A, Richomme P, Hensel A, Ganzera M (2020) Absolute configuration of mycosporine-like amino acids, their wound healing properties and in vitro anti-aging effects. Mar Drugs 18, 35 doi: 10.3390Y/md18010035

45. Volkmann M, Gorbushina AA, Kedar L, Oren A (2006) Structure of euhalothece-362, a novel red-shifted mycosporine-like amino acid, from halophilic cyanobacterium (*Euhalothece sp.*). FEMS Microbiol Lett 258:50-54

46. Tarasuntisuk S, Patipong T, Hibino T, Waditee-Sirisattha R, Kageyama H (2018) Inhibitory effects of mycosporine-2-glycine isolated from a halotolerant cyanobacterium on protein glycation and collagenase activity. Letters in Applied Microbiology 67: 314-320

47. White JD, Cammack JH, Sakuma K (1989) The synthesis and absolute configuration of Mycosporines, A novel application of the Staudinger Reaction. J Am Chem Soc 111:8970-8972

48. Frisch MJ, Trucks GW, Schlegel HB, Scuseria GE, Robb MA, Cheeseman JR, Scalmani G, Barone V, Mennucci B, Petersson GA, Nakatsuji H, Caricato M, Li X, Hratchian HP, Izmaylov AF, Bloino J, Zheng G, Sonnenberg JL, Hada M, Ehara M, Toyota K, Fukuda R, Hasegawa J, Ishida M, Nakajima T, Honda Y, Kitao O, Nakai H, Vreven T, Montgomery JA, Peralta JE, Ogliaro F, Bearpark M, Heyd JJ, Brothers E, Kudin KN, Staroverov VN, Kobayashi R, Normand J, Raghavachari K, Rendell A, Burant JC, Iyengar SS, Tomasi J, Cossi M, Rega N, Millam NJ, Klene M, Knox JE, Cross JB, Bakken V, Adamo C, Jaramillo J, Gomperts R, Stratmann RE, Yazyev O, Austin AJ, Cammi R, Pomelli C, Ochterski JW, Martin RL, Morokuma K, Zakrzewski VG, Voth GA, Salvador P, Dannenberg JJ, Dapprich S, Daniels AD, Farkas Ö, Foresman JB, Ortiz JV, Cioslowski J, Fox DJ (2009) Gaussian 09, Revision B01. Wallingford CT, Gaussian, Inc.

49. Furusaki A, Matsumoto T, Tsujino I, Sekikawa I (1980) The crystal and molecular structure of Palythine Trihydrate Bull Chem Soc Jpn 53:319-323

Tables

Due to technical limitations, table 1-2 is only available as a download in the Supplemental Files section.

Figures

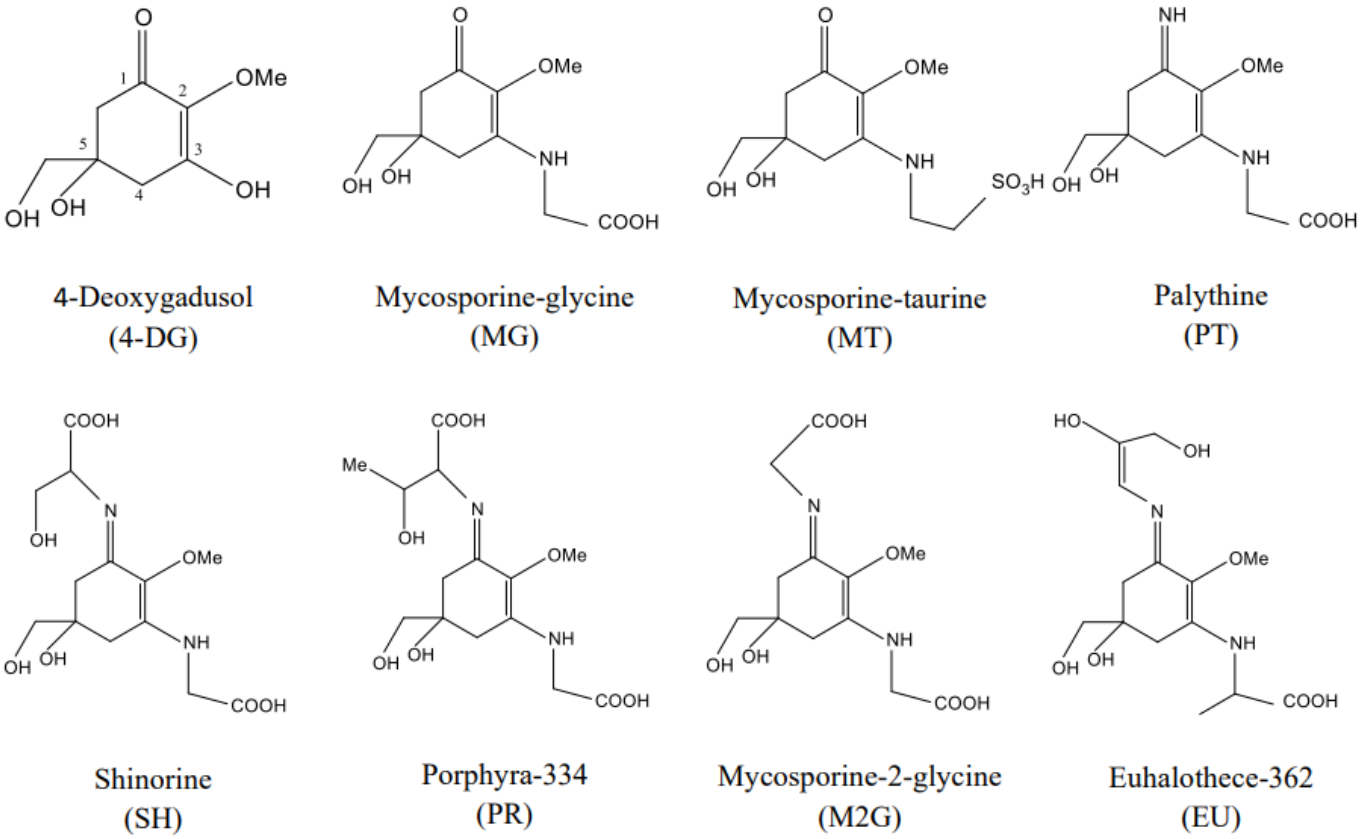

Figure 1

The precursor of all MAAs (4DG) and MAAs selected for this study

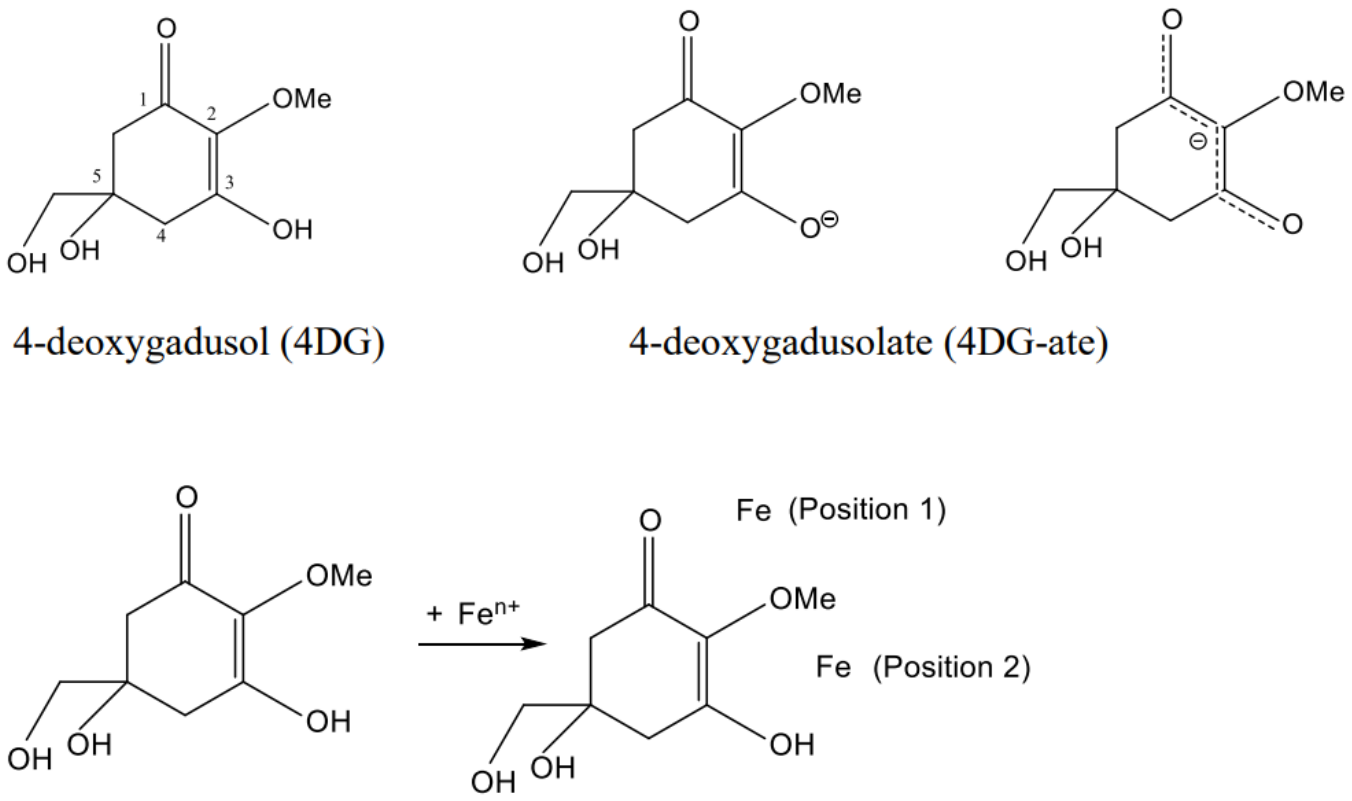

Figure 2

The neutral and anionic forms of 4DG, numbering sysem used throughout this work, available positions to place the iron (ferrous or ferric) ion

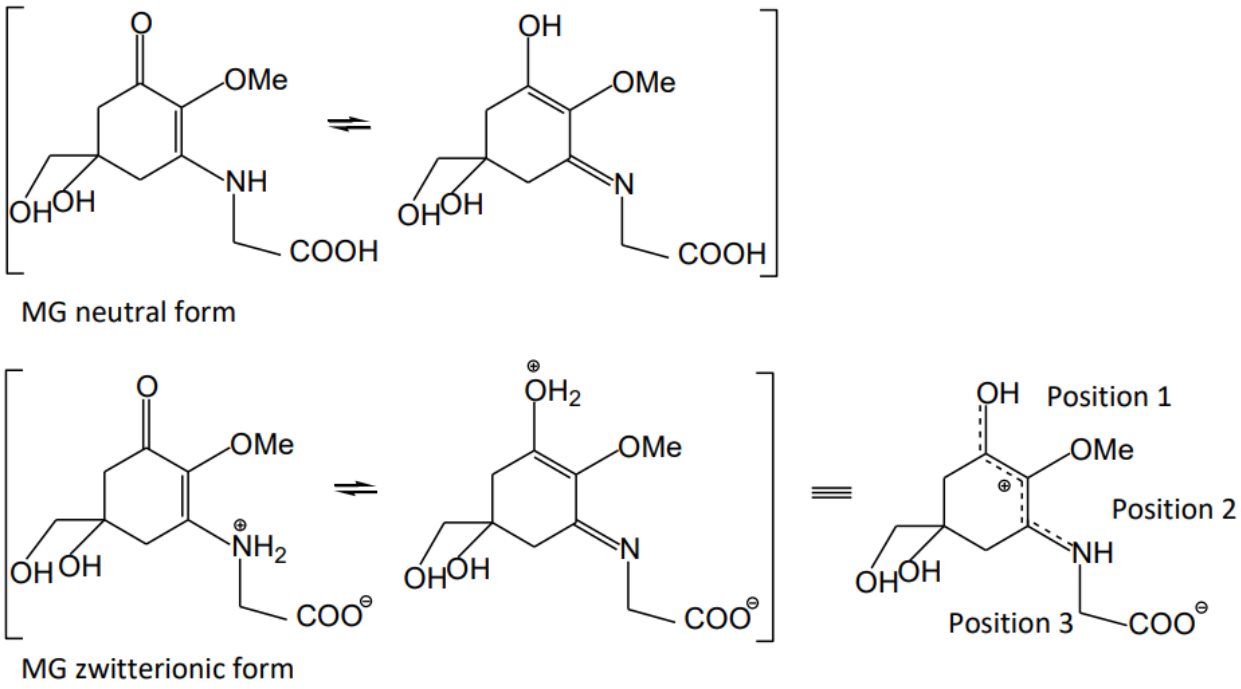

Figure 3

MG tautomers in the neutral form (above), the charge-resonance delocalized zwitterionic forms of MG and the three different positions tested for placing the iron (ferrous or ferric) ion

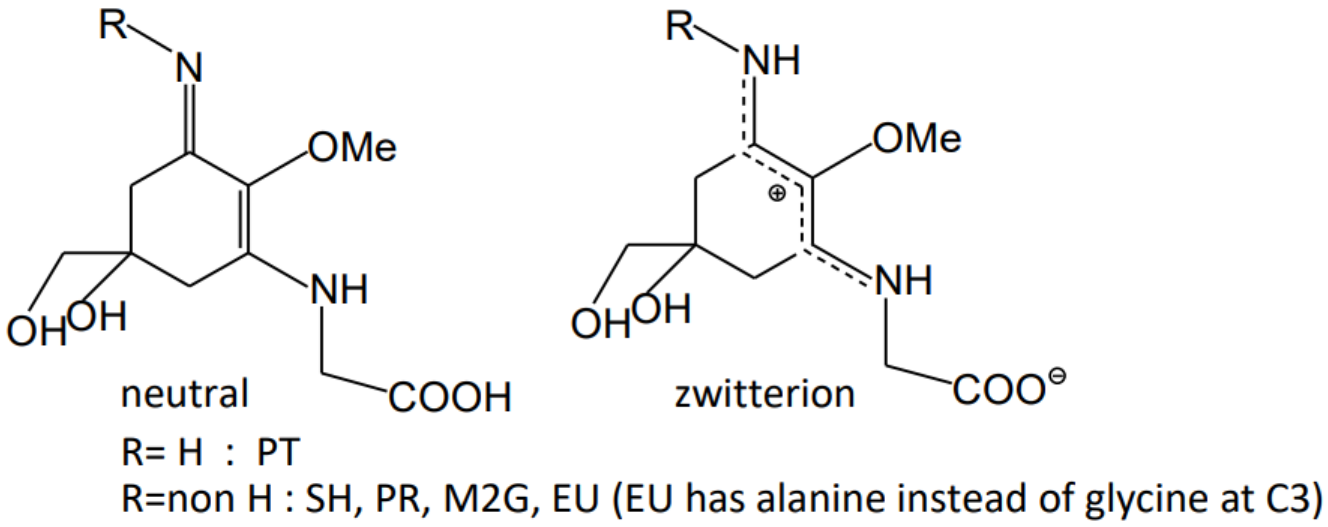

Figure 4

Neutral and zwitterionic forms for PT, SH, PR, M2G, and EU

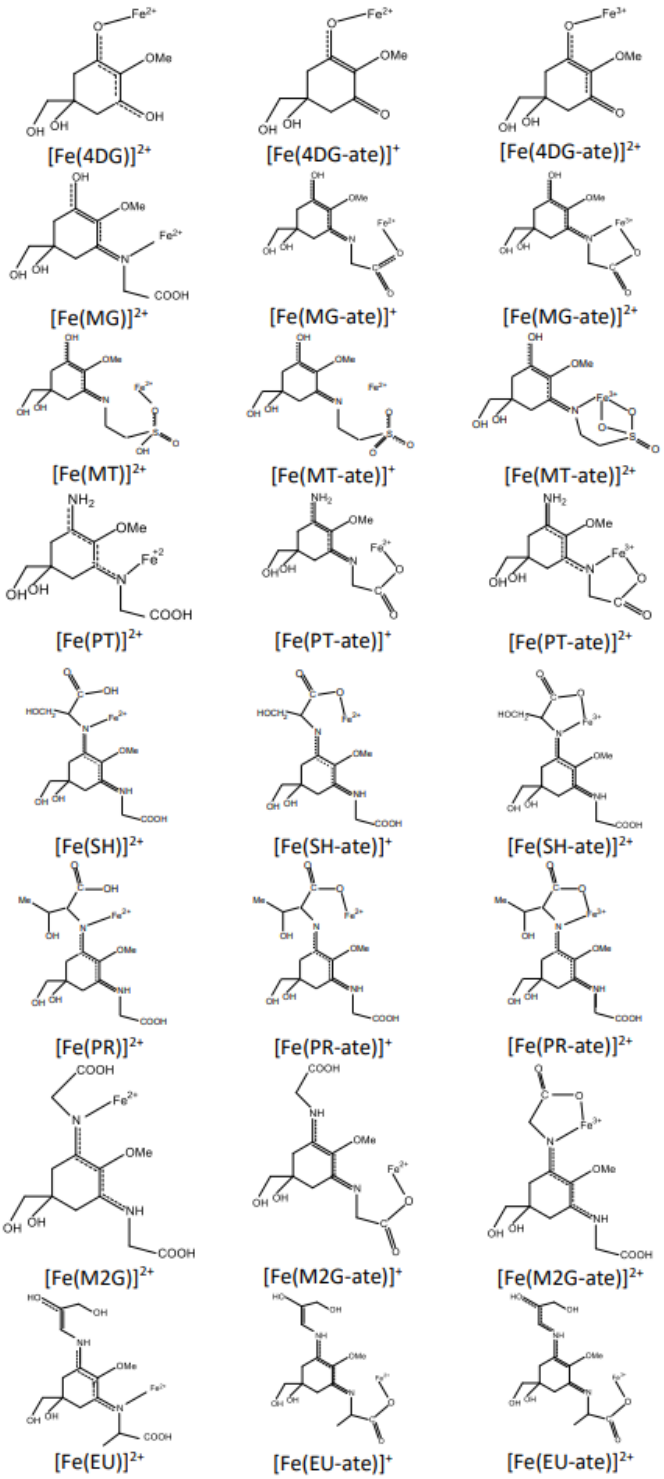

Figure 5

Representative drawings of the most stable iron chelates

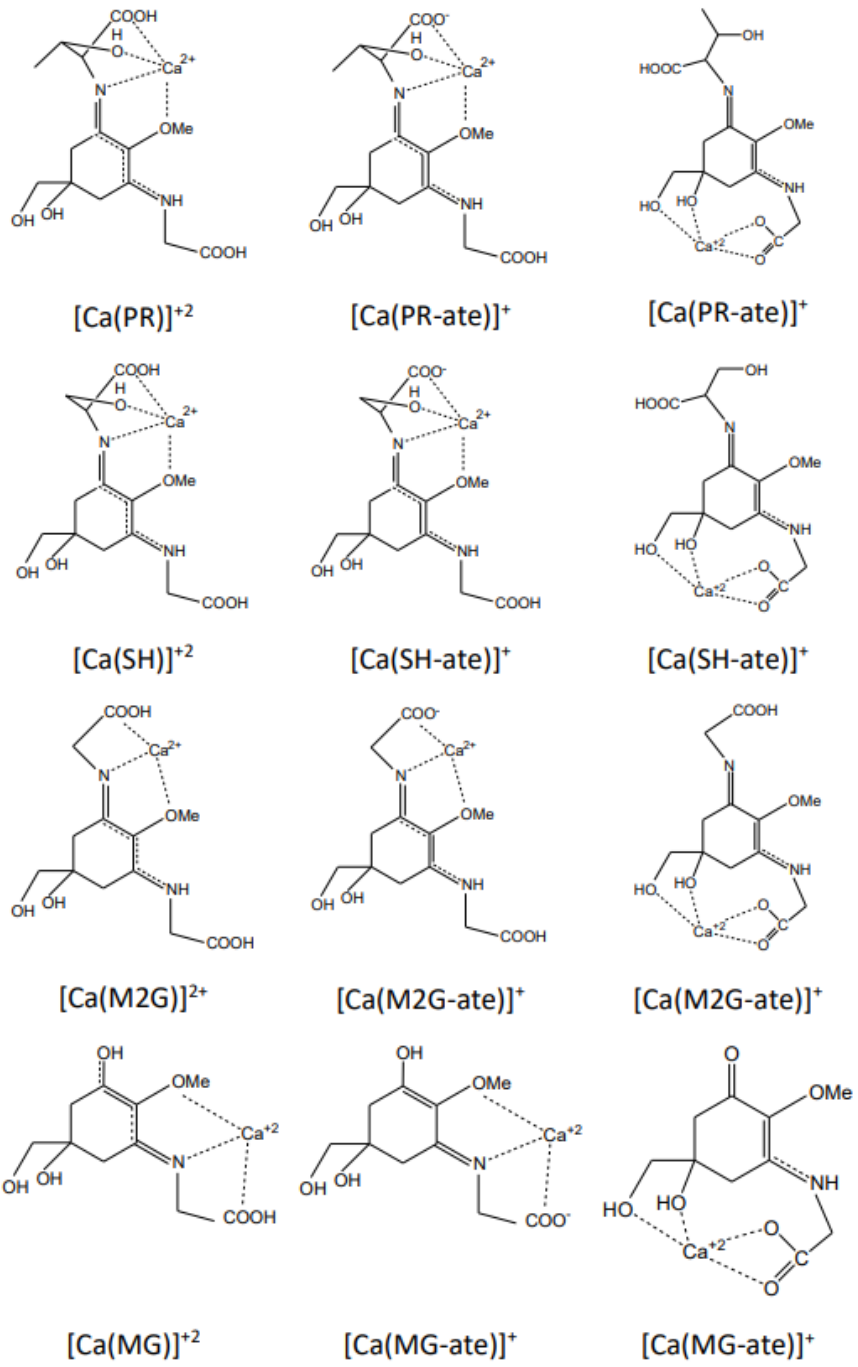

Figure 6

Representative drawings of the most stable calcium chelates

Supplementary Files

This is a list of supplementary files associated with this preprint. Click to download.

- Table1.pdf
- Table2.pdf
- TableS1.xlsx